Impact of panchromatic image characteristics on hyperspectral pansharpening: A case study in Agadir, Morocco

Volkan Yilmaz

Department of Geomatics Engineering, Karadeniz Technical University, Trabzon, Türkiye – volkanyilmaz.jdz@ktu.edu.tr

Keywords: Hyperspectral Pansharpening, Image Fusion, Spatial Enhancement, Hypersharpening, Data Fusion, PRISMA.

Abstract

This study evaluates the impact of different panchromatic (PAN) images with varying spatial resolutions on hyperspectral (HS) pansharpening performance. While PRISMA (Precursore Iperspettrale della Missione Applicativa) HS imagery provide valuable spectral information at 30-m resolution, many applications require higher spatial detail. Using PRISMA satellite imagery from Agadir, Morocco, the research systematically compares three different PAN sources: PRISMA's native 5-m PAN band, downsampled 10-m PRISMA PAN image, and Sentinel-2 (S2) derived 10-m PAN image. Six pansharpening algorithms were tested across two distinct sites (urban and mixed rural-urban): three conventional methods and three advanced methods. Pansharpening performance was evaluated through both qualitative assessment and quantitative metrics. The methodology considered how each algorithm handles the trade-off between spectral fidelity and spatial enhancement. Results demonstrated that PRISMA's native 5-m PAN consistently delivered superior results across metrics, particularly when pansharpened with advanced algorithms like MTF-GLP and MTF-GLP-HPM, which preserved spectral characteristics while enhancing spatial details. The 10-m PRISMA PAN showed moderate effectiveness, while S2 10-m PAN produced the least favourable outcomes due to limited spatial resolution and spectral compatibility. These findings emphasize the importance of selecting high-resolution PAN imagery from the same sensor platform when conducting HS pansharpening for environmental monitoring applications.

1. Introduction

Hyperspectral (HS) imaging is a crucial remote sensing tool due to its ability to capture narrowband spectral bands, which help extract valuable information from the Earth's surface. Recent technological innovations have enabled the design of cutting-edge satellites that provide high-quality HS imagery. HS imagery can be used for many purposes, including remote sensing of vegetation (Im and Jensen, 2008), agriculture and forestry applications (Adão et al., 2017), mineral exploration (Bedini, 2017), water quality monitoring (Liu et al., 2021), disease detection on tree leaves (Abdulridha et al., 2019), target detection (González et al., 2016), anomaly detection (Chand and Chiang, 2002) etc.

One of the most prominent HS imaging satellites today is PRISMA (Precursore Iperspettrale della Missione Applicativa), operated by the Italian Space Agency. PRISMA offers a HS image with 239 spectral bands (between 400 and 2500 nm) at 30 m, along with a panchromatic (PAN) band at a 5 m resolution. To date, PRISMA imagery have been used for many tasks, including water quality retrieval (Niroumand-Jadidi et al., 2020), mineral alteration mapping (Bedini and Chen, 2020), analysis and detection of wildfires (Spiller et al., 2021), forest type mapping (Vangi et al., 2021), retrieval of crop traits (Tagliabue et al., 2022), estimating soil organic carbon content (Golkar Amoli et al., 2024), monitoring habitat diversity (Laurin et al., 2025) etc.

While 30 m resolution provided by PRISMA imagery is suitable for many large-scale applications, it may not be sufficient for tasks requiring higher spatial detail. Image fusion provides a practical solution to this issue by enhancing the spatial features of HS imagery with finer spatial details of a higher-resolution image. This reference image could be PRISMA's 5-m PAN image or another high-resolution multispectral (MS)/PAN image. When an HS image is enhanced with a PAN image, the process is known as HS pansharpening. Qu et al., (2019) provided a clear visual representation of the HS pansharpening process, as illustrated in Figure 1.

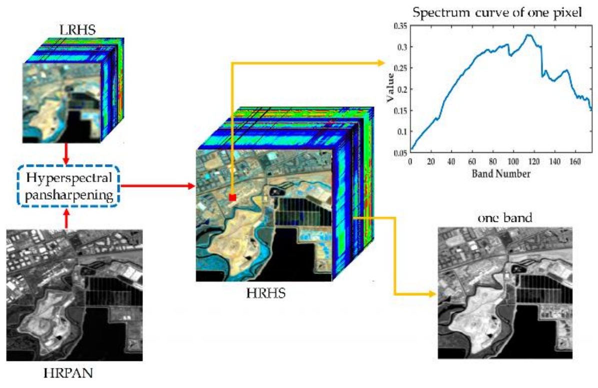

Figure 1. HS pansharpening concept (Qu et al., 2019).

HS pansharpening offers significant advantages by enhancing the spatial features of HS imagery while retaining their rich spectral information (Yilmaz, 2022). By fusing high-resolution PAN imagery with lower-resolution HS data, this technique enables detailed spatial analysis without sacrificing spectral depth. However, HS pansharpening also presents notable challenges. The vast number of spectral bands increases computational complexity and makes it difficult to maintain spectral fidelity during the fusion process (Yilmaz, 2022). Many pansharpening algorithms, originally developed for MS data, struggle with the high dimensionality and spectral correlation in HS datasets, often leading to spectral distortion. Moreover, the lack of standardized quality assessment metrics for HS fusion complicates the evaluation and comparison of different methods. Another key factor influencing the performance of HS pansharpening is the characteristics of the input PAN data used. Despite these drawbacks, ongoing research and advances in machine learning continue to improve the effectiveness of HS pansharpening techniques (Zini et al., 2024; Wang et al., 2024). In the light of all these, this study aims to analyse the influence of different PAN images with varying spatial resolutions on the performance of various HS pansharpening algorithms.

This study investigates how the integration of different PAN images with varying spatial resolutions influences the performance of HS pansharpening algorithms. By systematically analysing these effects, the research provides critical insights into optimal image fusion strategies. It not only advances the technical understanding of HS pansharpening but also informs best practices for leveraging satellite data like PRISMA in high-resolution environmental monitoring. Such findings are particularly valuable as more HS missions are launched, necessitating robust methods for maximizing the utility of the data they provide.

2. Method

2.1 Test Sites

The current study aimed at improving the spatial detail quality of a PRISMA HS image, which was acquired over Agadir on 31/01/2021. Agadir is a vibrant coastal city located in the southwest of Morocco, along the Atlantic Ocean. The experiments were carried out at two test locations in Agadir. Site 1 is an urban area, whereas Site 2 is a mix of urban and rural areas. Figure 2 shows the test sites.

Site 1

Site 2

Figure 2. Test sites.

2.2 HS Pansharpening

This study fused the PRISMA HS image with three PAN images using six different pansharpening algorithms. The first PAN image is the original 5-m resolution PAN band from the PRISMA satellite, the second is a downsampled 10 m version of the same image, and the third was generated by averaging the 10-m spectral bands of a Sentinel-2 (S2) image acquired on 10/03/2021. The used pansharpening algorithms included the three conventional methods, i.e., Modified Intensity-Hue-Saturation (MIHS) (Siddiqui, 2003), Gram-Schmidt Adaptive (GSA) (Aiazzi et al., 2007), Principal Component Analysis (PCA) (Chavez and Kwarteng, 1989); and three advanced methods, i.e., Morphological Half Gradient (MF-HG) (Restaino et al., 2016), Generalized Laplacian Pyramid (GLP) with Modulation Transfer Function (MTF) matched filter (MTF-GLP) (Aiazzi et al., 2006) and MTF-GLP with High-Pass Modulation (MTF-GLP-HPM) (Vivone et al., 2014).

The GSA approach produces simulated low-resolution PAN data by calculating a weighted average of the original HS bands, with the weights derived from a multivariate regression analysis between the HS and PAN images (Aiazzi et al., 2007). The GSA is widely regarded for its adaptability and its data-driven weighting strategy, which enables it to align well with the spectral characteristics of the input imagery. However, its performance heavily depends on the accuracy of the regression model and the alignment between PAN and HS images. Errors in these areas can propagate into the fusion process, affecting both spatial and spectral fidelity.

The MIHS method improves upon the traditional IHS-based approach, which replaces the source PAN image with the intensity component derived from an IHS transformation of a three-band MS image. Instead, MIHS accounts for spectral overlap among the source images (Siddiqui, 2003). MIHS addresses a critical shortcoming of the traditional IHS approach, its lack of spectral awareness. By incorporating spectral overlap, MIHS aims at producing pansharpened images with better colour consistency and reduced spectral distortion. However, like its predecessor, it may still be limited in applications involving a large number of bands, making it problematic for HS datasets.

The PCA technique replaces the PAN data with the first principal component from a PCA transformation of the HS data, and then reconstructs the pansharpened image using the inverse PCA transformation (Chavez and Kwarteng, 1989). PCA-based pansharpening is often favoured for its computational efficiency and straightforward implementation. It aims to effectively capture the dominant spatial patterns in the data. However, since the principal components are statistical abstractions and not physically tied to specific spectral features, the reconstructed image may suffer from spectral shifts or loss of detail in less dominant spectral bands.

The MF-HG algorithm uses morphological pyramids, a non-linear decomposition technique using morphological operators. It extracts spatial details through a morphological operator based on the difference between two half-gradients (Restaino et al., 2016). The MF-HG aims at enhancing spatial features, particularly in edge-rich areas, thanks to its nonlinear morphological processing. It may be particularly useful when fine textures and sharp transitions are crucial. However, its nonlinear nature may introduce challenges in maintaining spectral consistency, especially when merging with sensitive HS data.

The MTF-GLP method employs the sensor's MTF to create a GLP reduction filter, allowing selective injection of spatial details (Aiazzi et al., 2006). MTF-GLP stands out for its physically grounded approach, as it incorporates the actual response characteristics of the sensor. This offers more realistic and balanced fusion, particularly useful in operational remote sensing. However, it requires detailed knowledge of the sensor's MTF, which may not always be accessible or precise.

The MTF-GLP-HPM extends the MTF-GLP approach by incorporating the MTF prior to downsampling and employing a HPM injection technique, which enhances spatial details by multiplying spatial features (Vivone et al., 2014; Serifoglu Yilmaz and Gungor, 2023). MTF-GLP-HPM takes spatial detail enhancement a step further by adopting multiplicative modulation, which offers visibly sharper results. This makes it highly effective for applications requiring high spatial precision. However, the aggressive enhancement may sometimes lead to over-sharpening. Further information about these pansharpening techniques can be found in Serifoglu Yilmaz et al., (2022).

2.3 Quality Assessment

The pansharpened images were evaluated qualitatively and quantitatively. Similar to Yilmaz (2022), quantitative evaluation was done using the quality metrics Peak Signal-to-Noise Ratio PSNR (Yokoya et al., 2017), Spectral Angular Mapper (SAM) (Kruse et al., 1993), Erreur Relative Globale Adimensionnelle de Synthèse (ERGAS) (Wald, 2000) and $Q2^n$ (Garzelli and Nencini, 2009). ERGAS is calculated as (Wald, 2000);

$$ERGAS = 100r\sqrt{\frac{1}{B}\sum_{i=1}^{B}\frac{\|x_i - \hat{x}_i\|_2^2}{\left(\frac{1}{P}1_P^T x_i\right)^2}} \tag{1}$$

where, x_i is the reference data band, $\hat{x}_i$ is the fused band and r is the scale ratio between HS and PAN. Smaller values indicate better quality for ERGAS metric. PSNR is computed as (Yokoya et al., 2017);

$$PSNR = 10 \cdot \log_{10}\left(\frac{\max(x_i)^2}{\|x_i - \hat{x}_i\|_2^2/P}\right) \tag{2}$$

where, P is the total number of image bands. Larger values indicate better quality for PSNR metric. SAM is calculated as (Kruse et al., 1993; Serifoglu Yilmaz et al., 2019);

$$SAM = \arccos\left(\frac{x_j^T \hat{x}_j}{\|x_j\|_2 \|\hat{x}_j\|_2}\right) \tag{3}$$

Smaller values are optimum for SAM metric. $Q2^n$ metric, advanced version of the Universal Image Quality Index (UIQI) metric (Wang and Bovik, 2002), models each spectrum as a hypercomplex number as (Garzelli and Nencini, 2009);

$$\begin{gathered} Q2^n = x_{j,0} + x_{j,1}i_1 + x_{j,2}i_2 + \cdots + x_{j,2^n-1}i_{2^n-1} \\ UIQI = \frac{\sigma_{x\hat{x}}}{\sigma_x\sigma_{\hat{x}}} \cdot \frac{2\acute{x}\hat{\acute{x}}}{\acute{x}^2 + \hat{\acute{x}}^2} \cdot \frac{2\sigma_x\sigma_{\hat{x}}}{\sigma_x^2 + \sigma_{\hat{x}}^2} \end{gathered} \tag{4}$$

where, $\acute{x}$ and $\hat{\acute{x}}$ stand for the mean of x and $\hat{x}$, respectively (Yilmaz, 2022). Larger values signify better quality for $Q2^n$ metric.

3. Results

3.1 Qualitative Assessment

Figures 3 and 4 show the input images and resulting pansharpened images in RGB band combination for Sites 1 and 2, respectively. As seen in the figures, in both sites, all methods produced blur effect on resulting images to some degree. This is expected as pansharpening methods involve some trade-off between spectral and spatial fidelity (Yilmaz et al., 2021).

3.1.1 Site 1: Among the three PAN sources, the results obtained using PRISMA 5-m PAN exhibited the best balance between spatial detail and spectral fidelity. Especially for the more advanced pansharpening methods like MTF-GLP-HPM and MTF-GLP, the results are noticeably sharp and preserve the original colours quite well. These methods managed to enhance spatial resolution effectively while minimizing spectral distortion, making them excellent choices when using the high-resolution 5-m PAN. Even the simpler methods like GSA and PCA perform decently, they started to introduce some colour distortions or lose a bit of sharpness. Overall, the PRISMA 5-m PAN produced the most visually satisfying results among all imagery.

With the PRISMA 10-m PAN, there is a noticeable decline in spatial sharpness across all methods compared to the 5-m PAN. While the colour fidelity is somewhat preserved, especially with GSA and MF-HG, the enhancement in spatial detail is less convincing. Techniques like MTF-GLP-HPM still showed improvements, but the results appear less crisp than their counterparts fused with the 5-m PAN. This suggests that the PRISMA 10-m PAN lacks sufficient resolution to make a strong impact in sharpening while maintaining the HS image's colour characteristics.

Fusion results obtained with S2 10-m PAN showed the weakest performance overall. Both colour fidelity and spatial detail are compromised in most pansharpening methods. The colour deviation is more significant in pansharpening techniques like IHS and PCA, which introduced noticeable spectral distortions. Even advanced methods like MTF-GLP and MTF-GLP-HPM failed to recover adequate sharpness from the S-2 PAN input. This indicates that the Sentinel-2 PAN image may not be as compatible or effective as PRISMA's native PAN image for HS pansharpening purposes.

In the Site 1, the best pansharpening results were clearly achieved when using PRISMA 5-m PAN, particularly with the MTF-GLP-HPM and MTF-GLP methods. These provided a solid trade-off between spatial detail and spectral fidelity. The PRISMA 10-m PAN delivered moderate improvements but fell short in sharpness. S-2 10-m PAN resulted in lower quality pansharpened images, indicating it is less suitable for enhancing PRISMA HS data.

Site 2: Just like in Figure 3, the pansharpening results obtained using the PRISMA 5-m PAN are the strongest in Figure 4 as well. The MTF-GLP-HPM and MTF-GLP delivered excellent visual results; sharp, well-defined features with minimal colour distortion. These methods successfully brought out the fine spatial features from the higher-resolution PAN, while keeping the HS image's colour characteristics largely intact. Even the methods like GSA and MF-HG performed quite well, offering solid enhancements in spatial detail with manageable colour shifts.

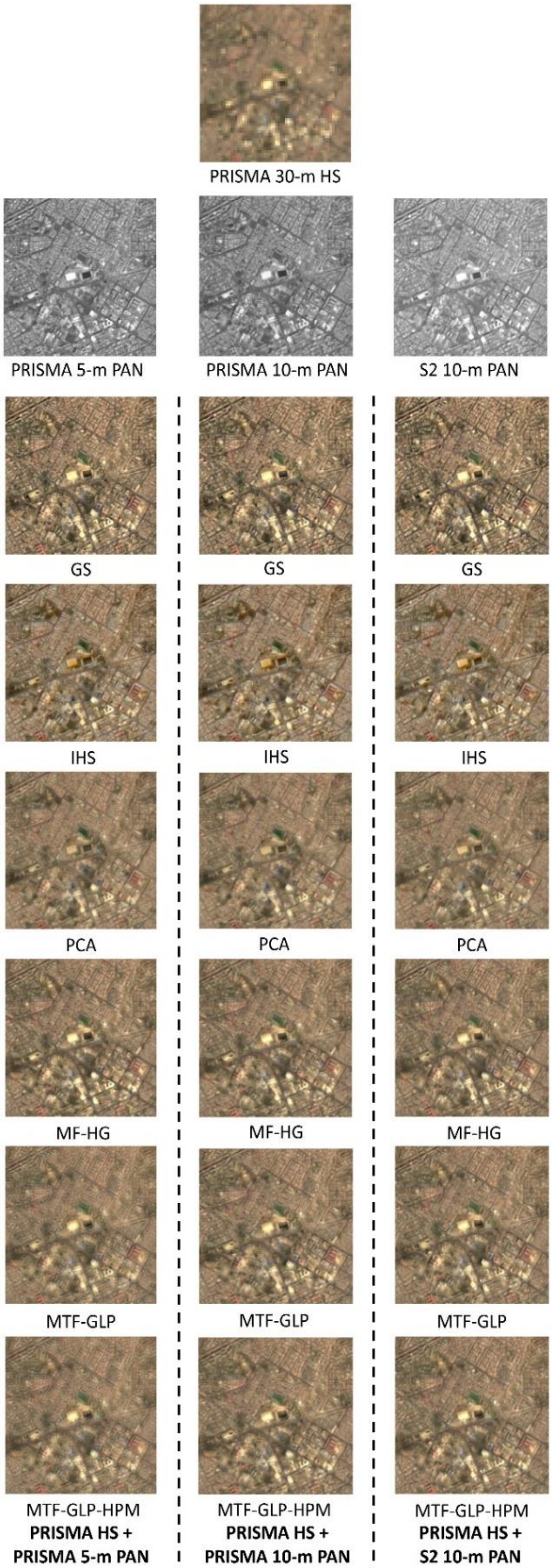

Figure 3. Pansharpened images produced for site 1.

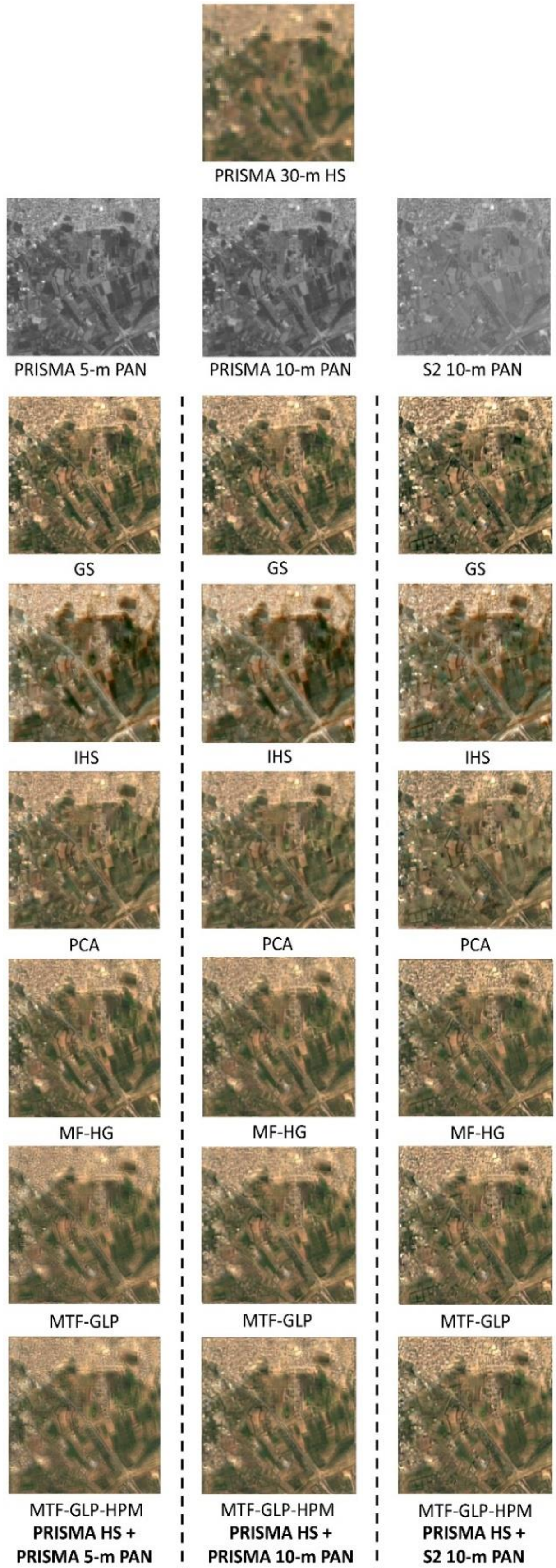

Figure 4. Pansharpened images produced for site 2.

https://doi.org/10.5194/isprs-archives-XLVIII-4-W17-2025-401-2026

When using PRISMA 10-m PAN, the quality of the pansharpening results was notably diminished compared to the 5-m PAN. There is a modest improvement in spatial sharpness over the original HS image, but it is not as prominent. Colour fidelity was somewhat preserved, with methods like MF-HG and GSA retaining decent spectral accuracy. However, sharpness was visibly reduced across all methods, even in MTF-GLP-HPM, which suggests that the 10-m spatial resolution of the PAN data is a limiting factor in achieving crisp outputs.

The results obtained with S2 10-m PAN showed the most degradation in both spatial detail and colour quality. Most methods introduced notable spectral distortion, especially IHS and PCA, which tend to oversaturate or shift colours away from the original HS appearance. Moreover, spatial sharpening was weak, edges were poorly defined, and textures were soft. Even the advanced methods like MTF-GLP-HPM and MTF-GLP could not compensate for the lower quality of the S2 10-m PAN image. This further reinforces that S2 10-m PAN is not well-suited for this type of high-fidelity fusion.

Figure 4 also supports the conclusion that PRISMA 5-m PAN was the most effective PAN input for enhancing HS data, producing higher-quality results especially when fused with MTF-GLP-HPM or MTF-GLP. PRISMA 10-m PAN provided some value but lacked the resolution to significantly sharpen the image. Sentinel-2 10-m PAN, on the other hand, led to visibly worse results, making it the least suitable option for high-quality pansharpening in this context.

Site	Dataset	Method	PSNR	SAM	ERGAS	$Q2^n$
1	Prisma HS - Prisma 5 m PAN	**GSA**	**29.1267**	1.2828	**1.7305**	**0.6234**
		IHS	**24.9961**	**1.0694**	**2.6262**	**0.3318**
		PCA	**25.2202**	**0.7045**	**2.4460**	**0.2926**
		MF-HG	28.6952	0.4762	**1.6416**	0.5575
		MTF-GLP	**36.6429**	**0.3826**	**0.6511**	**0.8494**
		MTF-GLP-HPM	**36.6016**	**0.3770**	**0.6555**	**0.8366**
	Prisma HS - Prisma 10 m PAN	**GSA**	28.7303	1.3740	3.0409	0.6065
		IHS	24.7453	1.1015	4.5074	0.3259
		PCA	24.9751	0.7189	4.1935	0.2882
		MF-HG	**30.1725**	**0.4508**	2.3122	**0.6364**
		MTF-GLP	31.7832	0.4410	1.9012	0.7320
		MTF-GLP-HPM	31.6588	0.4237	1.9308	0.7001
	Prisma HS - S2 10 m PAN	**GSA**	26.6291	**1.2606**	3.6712	0.5073
		IHS	24.6214	1.0867	4.5719	0.3203
		PCA	24.8779	0.7071	4.2407	0.2921
		MF-HG	30.0319	0.4516	2.3545	0.6096
		MTF-GLP	31.5240	0.4381	1.9589	0.7030
		MTF-GLP-HPM	31.4903	0.4247	1.9701	0.6730
2	Prisma HS - Prisma 5 m PAN	**GSA**	27.2648	**3.5051**	**2.3289**	**0.5968**
		IHS	21.7014	1.8951	**3.5383**	0.3388
		PCA	**26.2304**	**4.4613**	**3.0158**	**0.5285**
		MF-HG	26.2580	1.1193	**1.9733**	0.6182
		MTF-GLP	**35.4548**	**0.5322**	**0.6736**	**0.8614**
		MTF-GLP-HPM	**35.6130**	**0.5394**	**0.6754**	**0.8554**
	Prisma HS - Prisma 10 m PAN	**GSA**	26.9794	3.6394	3.9978	0.5829
		IHS	21.5995	1.9169	5.9683	0.3309
		PCA	26.0660	4.5553	5.1329	0.5190
		MF-HG	**28.4039**	**0.9225**	2.5812	**0.6824**
		MTF-GLP	29.9701	0.7778	2.1015	0.7357
		MTF-GLP-HPM	30.0388	0.7872	2.1235	0.7304
	Prisma HS - S2 10 m PAN	**GSA**	**28.0158**	3.6107	5.1653	0.4671
		IHS	**22.3578**	**1.6289**	5.4638	**0.3587**
		PCA	24.6029	5.5691	6.1647	0.4506
		MF-HG	27.2374	1.0168	2.9789	0.6212
		MTF-GLP	28.5140	0.8402	2.4784	0.6863
		MTF-GLP-HPM	28.7140	0.8756	2.4970	0.6697

Table 1. Quality metric values determined for test sites.

https://doi.org/10.5194/isprs-archives-XLVIII-4-W17-2025-401-2026 | © Author(s) 2026. CC BY 4.0 License.

3.2 Quantitative Assessment

Slight differences between the source images and the pansharpened imagery may be difficult to discern visually, which is the case for the pansharpened images given in Figures 3 and 4. To better assess the quality of the pansharpened imagery, PSNR, SAM, ERGAS and $Q2^n$ metrics were determined using the pansharpened imagery and source imagery. Table 1 shows the calculated metric values. In the table, the best metric values calculated from all resulting images obtained using three different input datasets are highlighted in bold.

3.2.1 Site 1: At Site 1, 5-m PRISMA PAN consistently produced the most favourable pansharpening outcomes across all evaluated metrics. The MTF-GLP and MTF-GLP-HPM methods yielded the highest PSNR values, 36.6429 and 36.6016 respectively, indicating superior preservation of details. These methods also resulted in the lowest SAM (0.3826-0.3770) and ERGAS (0.6511-0.6555) values, implying minimal distortion. Furthermore, the $Q2^n$ values for these methods exceeded 0.83, highlighting better overall quality of the fused image. These results strongly indicate that the finer-resolution 5 m PAN image from PRISMA significantly enhances the quality of pansharpened output.

10-m PRISMA PAN, although slightly coarser in resolution, showed comparatively strong performance. For MTF-GLP and MTF-GLP-HPM, it achieved PSNR values over 31 and $Q2^n$ values around 0.70-0.73. However, the spectral and spatial fidelity, as indicated by ERGAS and SAM values, were marginally inferior to those obtained using the 5-m PRISMA PAN image. This suggests that while 10-m PRISMA PAN image can serve as a viable alternative for pansharpening, its efficacy diminishes slightly due to its lower spatial resolution.

In contrast, 10-m S2 PAN data yielded the least favourable results. Despite the application of sophisticated methods, such as MTF-GLP-HPM, the PSNR remained under 31.5, and $Q2^n$ values did not exceed 0.7030. SAM and ERGAS values were also noticeably higher compared to Prisma-derived PAN images, indicating reduced image quality. These findings demonstrate that 10-m S2 PAN image is less suitable for high-quality HS pansharpening at this site.

3.2.2 Site 2: The trends observed at Site 1 were largely consistent with those at Site 2, reinforcing the superiority of high-resolution PAN images. The 5-m PRISMA PAN again outperformed all other datasets. Specifically, MTF-GLP-HPM and MTF-GLP returned PSNR values above 35, while SAM and ERGAS values remained impressively low (SAM $\approx$ 0.53, ERGAS $\approx$ 0.67). Notably, $Q2^n$ values reached up to 0.8614, representing the highest spatial-spectral quality score across both sites. These outcomes underscore the substantial advantage conferred by high-resolution PAN data in retaining both spatial sharpness and spectral integrity.

10-m PRISMA PAN image again demonstrated respectable performance in Site 2. For example, MTF-GLP-HPM achieved a PSNR of 30.0388, SAM of 0.7872, ERGAS of 2.1235, and $Q2^n$ of 0.7304. These values suggest that while 10-m PRISMA PAN image is a viable choice, its effectiveness is still slightly compromised in comparison to its 5 m counterpart.

10-m S2 PAN data continued to exhibit the weakest performance across all metrics in Site 2 as well. Even under optimal conditions using MTF-GLP-HPM, the highest PSNR achieved was 28.7140, and $Q2^n$ remained below 0.69. Moreover, SAM and ERGAS values were considerably higher, indicating increased image distortion. This performance degradation likely stems from the lower spatial resolution and spectral compatibility between Sentinel-2 PAN image and HS data.

4. Conclusion

A holistic examination across both sites revealed that 5-m PRISMA PAN image provided the most accurate and reliable base for pansharpening, particularly when used with sophisticated fusion methods like MTF-GLP-HPM and MTF-GLP. These techniques consistently delivered superior results in all quality metrics, outperforming both 10-m PRISMA PAN and 10-m S2 PAN alternatives. The 10-m PRISMA PAN, while effective, represented a moderate compromise between quality and availability, and may be appropriate in cases where higher-resolution PAN data is unavailable. Meanwhile, the 10-m S2 PAN demonstrated limited effectiveness, with performance constraints likely due to its coarser spatial resolution.

To identify the best and worst performing pansharpening approach, a performance score ranging from 1 to 6 was assigned to each pansharpened image, as also done by Yilmaz et al., (2020) and Serifoglu Yilmaz et al., (2020), based on the quality metric values (with six pansharpening methods in total). During scoring, higher quality metric values received higher scores. The average scores for the pansharpening techniques are displayed in Figure 5. As illustrated in the figure, the advanced pansharpening methods, MTF-GLP and MTF-GLP-HPM, demonstrated the best performance, while the traditional methods, PCA and IHS, delivered the poorest results.

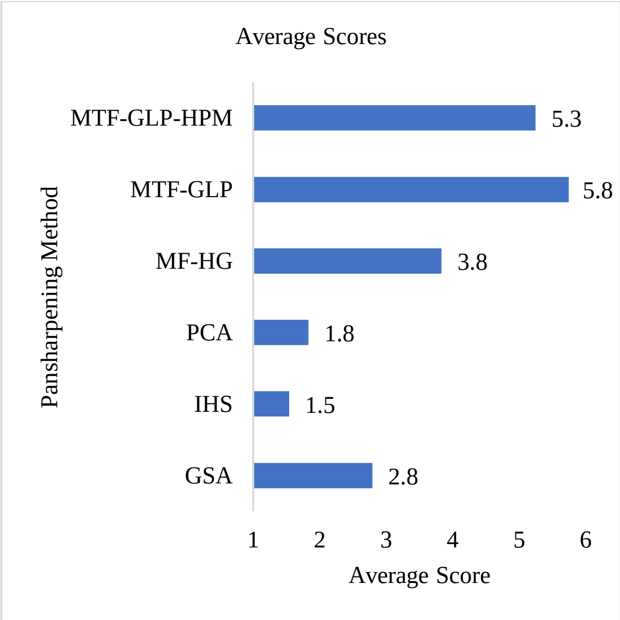

Figure 5. Average performance scores computed for pansharpening methods.

The results emphasize the importance of selecting higher-resolution PAN data and appropriate fusion algorithm to maximize the quality of pansharpened HS products. These findings hold implications for remote sensing applications that need high-fidelity spectral and spatial data integration, such as precision agriculture, urban monitoring, and environmental assessment.

References

Abdulridha, J., Batuman, O., Ampatzidis, Y., 2019. UAV-based remote sensing technique to detect citrus canker disease utilizing hyperspectral imaging and machine learning. *Remote Sensing* 11(11), 1373.

Adão, T., Hruška, J., Pádua, L., Bessa, J., Peres, E., Morais, R., Sousa, J.J., 2017. Hyperspectral imaging: A review on UAV-based sensors, data processing and applications for agriculture and forestry. *Remote Sensing* 9(11), 1110.

Aiazzi, B., Alparone L., Baronti S., Garzelli, A., Selva M., 2006. MTF tailored multiscale fusion of high-resolution MS and Pan imagery. *Photogrammetric Engineering & Remote Sensing* 72(5), 591-596.

Aiazzi, B., Baronti, S., Selva, M., 2007. Improving component substitution pansharpening through multivariate regression of MS+Pan data. *IEEE Transactions on Geoscience and Remote Sensing*, 45(10), 3230-3239.

Bedini, E., 2017. The use of hyperspectral remote sensing for mineral exploration: A review. *Journal of Hyperspectral Remote Sensing* 7(4), 189-211.

Bedini, E., Chen, J., 2020. Application of PRISMA satellite hyperspectral imagery to mineral alteration mapping at Cuprite, Nevada, USA. *Journal of Hyperspectral Remote Sensing* 10(2), 87-94.

Chang, C.I., Chiang, S.S., 2002. Anomaly detection and classification for hyperspectral imagery. *IEEE Transactions on Geoscience and Remote Sensing* 40(6), 1314-1325.

Chavez, A., Kwarteng, P., 1989. Extracting spectral contrast in Landsat Thematic Mapper image data using selective principal component analysis. *Photogrammetric Engineering & Remote Sensing* 55(3), 339-348.

Garzelli, A., Nencini, F., 2009. Hypercomplex Quality Assessment of Multi/hyperspectral Images. *IEEE Geoscience and Remote Sensing Letters* 6(4), 662-665.

Golkar Amoli, M., Hasanlou, M., Taghizadeh Mehrjardi, R., Samadzadegan, F., 2024. Exploring the Potential of PRISMA Satellite Hyperspectral Image for Estimating Soil Organic Carbon in Marvdasht Region, Southern Iran. *Remote Sensing* 16(12), 2149.

González, C., Bernabé, S., Mozos, D., Plaza, A., 2016. FPGA implementation of an algorithm for automatically detecting targets in remotely sensed hyperspectral images. *IEEE Journal of Selected Topics in Applied Earth Observations and Remote Sensing* 9(9), 4334-4343.

Im, J., Jensen, J.R., 2008. Hyperspectral remote sensing of vegetation. *Geography Compass* 2(6), 1943-1961.

Kruse, F.A., Lefkoff, A.B., Boardman, J.W., Heidebrecht, K.B., Shapiro, A.T., Barloon, P.J., Goetz, A.F.H., 1993. The Spectral Image Processing System (Sips)—interactive Visualization and Analysis of Imaging Spectrometer Data. *Remote Sensing of Environment* 44(2-3), 145–163.

Laurin, G. V., Zabeo, C., Giuliarelli, D., Tesfamariam, B. G., Cotrina-Sanchez, A., Valentini, R., Tufail, B., Ventura, B., Calfapietra, C., Barbati, A., 2025. Monitoring habitat diversity with PRISMA hyperspectral and lidar-derived data in Natura 2000 sites: Case study from a Mediterranean forest. *Ecological Indicators* 172, 113254.

Liu, H., Yu, T., Hu, B., Hou, X., Zhang, Z., Liu, X., Liu, J., Wang, X., Zhong, J., Tan, Z., Xia. S., Qian, B., 2021. UAV-Borne Hyperspectral Imaging Remote Sensing System Based on Acousto-Optic Tunable Filter for Water Quality Monitoring. *Remote Sensing* 13(20), 4069.

Niroumand-Jadidi, M., Bovolo, F., Bruzzone, L., 2020. Water quality retrieval from PRISMA hyperspectral images: First experience in a turbid lake and comparison with sentinel-2. *Remote Sensing* 12(23), 3984.

Qu, J., Li, Y., Du, Q., Dong, W., Xi, B., 2019. Hyperspectral pansharpening based on homomorphic filtering and weighted tensor matrix. *Remote Sensing* 11(9), 1005.

Restaino, R., Vivone, G., Dalla Mura, M., Chanussot, J., 2016. Fusion of multispectral and panchromatic images based on morphological operators. *IEEE Transactions on Image Processing* 25(6), 2882-2895.

Serifoglu Yilmaz, C., Gungor, O., 2023. A Metaheuristic Optimization-Based Solution to MTF-GLP-Based PANsharpening. *PFG–Journal of Photogrammetry, Remote Sensing and Geoinformation Science* 91(4), 245-272.

Serifoglu Yilmaz, C., Yilmaz, V., Güngör, O., 2020. On the use of the SOS metaheuristic algorithm in hybrid image fusion methods to achieve optimum spectral fidelity. *International Journal of Remote Sensing* 41(10), 3993-4021.

Serifoglu Yilmaz, C., Yilmaz, V., Gungor, O., 2022. A theoretical and practical survey of image fusion methods for multispectral pansharpening. *Information Fusion* 79, 1-43.

Serifoglu Yilmaz, C., Yilmaz, V., Gungor, O., Shan, J., 2019. Metaheuristic pansharpening based on symbiotic organisms search optimization. *ISPRS Journal of Photogrammetry and Remote Sensing* 158, 167-187.

Siddiqui, Y., 2003. The modified IHS method for fusing satellite imagery. in: Proc. *ASPRS 2003 Annual Conference*, Anchorage, Alaska, pp. 5-9.

Spiller, D., Ansalone, L., Amici, S., Piscini, A., Mathieu, P.P., 2021. Analysis and detection of wildfires by using prisma hyperspectral imagery. *The International Archives of Photogrammetry, Remote Sensing and Spatial Information Sciences* 43, 215-222.

Tagliabue, G., Boschetti, M., Bramati, G., Candiani, G., Colombo, R., Nutini, F., Pompilio, L., Rivera-Caicedo, J.P., Rossi, M., Rossini, M., Verrelst, J., Panigada, C., 2022. Hybrid retrieval of crop traits from multi-temporal PRISMA hyperspectral imagery. *ISPRS Journal of Photogrammetry and Remote Sensing* 187, 362-377.

Vangi, E., D'Amico, G., Francini, S., Giannetti, F., Lasserre, B., Marchetti, M., Chirici, G., 2021. The new hyperspectral satellite PRISMA: Imagery for forest types discrimination. *Sensors* 21(4), 1182.

This contribution has been peer-reviewed.
https://doi.org/10.5194/isprs-archives-XLVIII-4-W17-2025-401-2026

Vivone, G., Restaino, R., Dalla Mura M., Licciardi G., Chanussot J., 2014. Contrast and error-based fusion schemes for multispectral image pansharpening. *IEEE Geoscience and Remote Sensing Letters* 11(5), 930-934.

Wald, L., 2000. Quality of High Resolution Synthesised Images: Is There a Simple Criterion?" In Third conference" *Fusion of Earth data: merging point measurements, raster maps and remotely sensed images*, 99-103. Sophia Antipolis, France.

Wang, H., Zhang, J., Huo, L.Z., 2024. Multiscale hyperspectral pansharpening network based on dual pyramid and transformer. *IEEE Journal of Selected Topics in Applied Earth Observations and Remote Sensing* 17, 19786-19797.

Wang, Z., Bovik, A.C., 2002. A Universal Image Quality Index. *IEEE Signal Processing Letters* 9(3), 81-84.

Yilmaz, V., 2022. A comprehensive investigation of image fusion methods for spatial enhancement of hyperspectral images. *International Journal of Remote Sensing* 43(11), 4151-4186.

Yilmaz, V., Serifoglu Yilmaz, C., Gungor, O., 2021. Genetic algorithm-based synthetic variable ratio image fusion. *Geocarto International* 36(9), 989-1006.

Yilmaz, V., Serifoglu Yilmaz, C., Güngör, O., Shan, J., 2020. A genetic algorithm solution to the gram-schmidt image fusion. *International Journal of Remote Sensing* 41(4), 1458-1485.

Yokoya, N., Grohnfeldt, C., Chanussot, J., 2017. Hyperspectral and Multispectral Data Fusion: A Comparative Review of the Recent Literature. *IEEE Geoscience and Remote Sensing Magazine* 5(2), 29-56.

Zini, S., Barbato, M., Piccoli, F., Napoletano, P., 2024. Deep Learning Hyperspectral Pansharpening on Large-Scale PRISMA Dataset. *Remote Sensing* 16(12), 1-21.